



CENTRE DE RECERCA MATEMÀTICA

Title: *Contact melting of a rectangular block with temperature-dependent properties*
Journal Information: *International Journal of Thermal Sciences*,
Author(s): Cregan V., Williams J., Myers T.G..
Volume, pages: 150 1, DOI:[10.1016/j.ijthermalsci.2019.106218]



Contact melting of a rectangular block with temperature-dependent properties

V. Cregan^{a,*}, J. Williams^b, T.G. Myers^c

^a Department of Mathematics, Cork Institute of Technology, Cork, Ireland

^b School of Mathematical Sciences, Queen Mary University of London, United Kingdom

^c Centre de Recerca Matemàtica, Campus de Bellaterra Edifici C, 08193 Bellaterra, Barcelona, Spain

ARTICLE INFO

Keywords:

Phase change material
Contact melting
Heat balance integral method
Temperature-dependent properties

ABSTRACT

We consider a model for the contact melting of a block of phase change material on a flat, heated surface. The block and melt have linear temperature-dependent thermal conductivity and viscosity. The model consists of heat equations for the solid and liquid temperatures, the Navier–Stokes equations in the liquid melt layer, a Stefan condition at the solid–liquid interface and a force balance between the weight of the solid and the countering pressure in the liquid. The heat balance integral method is used to obtain an approximate solution for the solid temperature. We demonstrate that in the case of n-octadecane the inclusion of temperature-dependent effects slows down the melting process. Finally, we vary the parameters in the linear expressions for the conductivities and viscosities to understand the behaviour of the system.

1. Introduction

As a phase change material (PCM) melts, it absorbs energy in the form of latent heat. Conversely, as it freezes, energy is released into the surroundings. These properties have led to PCMs being used in applications such as the transportation of temperature sensitive materials (e.g., food, pharmaceutical products and electrical components), thermal energy storage systems in buildings [1,2], high-performance textiles [3,4] and solar energy-related applications [5,6]. Contact melting occurs when a PCM is placed in contact with a surface that is maintained above the PCM melt temperature. The solid begins to melt so that a thin liquid layer develops between the two surfaces. The weight of the solid acts to squeeze out the liquid, and thus the melt layer remains thin.

Theoretical descriptions for contact melting subject to constant material properties have been studied extensively. Moallemi et al. [7] performed experiments and presented a model which included a heat equation for the liquid temperature, equations of motion for flow in the melt layer, a Stefan condition at the solid–liquid interface and a force balance between the weight of the solid and the countering pressure in the liquid. To make analytical progress they assumed that the liquid temperature could be approximated by a quadratic function in the vertical coordinate. Their solutions for the solid height and melting velocity were in good qualitative agreement with data for n-octadecane. Bejan [8,9] obtained a linear approximation for the liquid temperature by neglecting the terms for convection and internal heat generation

due to liquid friction and retaining only the vertical thermal diffusion term. The solid temperature was fixed at the melt temperature. The liquid height could then be easily calculated via a standard one-phase Stefan model. The remaining unknown, the melt speed, was obtained by solving the equations of motion and the vertical force balance equation for the liquid pressure. Bejan [8] also modified the static contact melting problem to consider the case where the lower surface is moving at a constant horizontal velocity and melting arises due to friction. Hirata et al. [10] performed experiments on blocks of ice and n-octadecane with different aspect ratios. Solutions were obtained via Nusselt's liquid film theory and an iterative method was used to calculate the PCM mass at each step of the melt process.

To reduce model complexity, the above studies and many others use simplifying assumptions. These include:

- (1) an isothermal, solid fixed at the melt temperature, T_m ;
- (2) a quasi-steady melting process, where the melt front is fixed;
- (3) heat transfer in the liquid is dominated by conduction across the melt layer;
- (4) the lubrication approximation applies in the liquid layer;
- (5) the amount of melted liquid is small relative to that of the initial solid;
- (6) perfect thermal contact at the substrate–liquid interface;
- (7) the problem is two-dimensional.

* Corresponding author.

E-mail address: vincent.cregan@cit.ie (V. Cregan).

Following the above studies, there have been many extensions and refinements to the contact melting model. Listek and Bejan [11] removed assumption (1) by including a convective term in the heat equation for the solid. This results in an unrealistic, constant temperature gradient at the solid–liquid interface. Hong and Saito [12] neglected (2) and used a numerical algorithm to investigate the rapid rise of the liquid height at the onset of melting. Similarly, Yoo [13] also removed (2) and presented approximate analytical solutions for a three-dimensional model. Lacroix [14] proposed an analytical solution for the melting of a three-dimensional block that included varying solid temperature and mass (thus neglecting (1), (2), (5) and (7)). However, as outlined in [15], there are several inconsistencies in Lacroix's approach (i.e., the “constant” of separation that arises from separation of variables is time-dependent). To remove (3), Groulx and Lacroix [16] included the vertical convection term in the model. This approach required a value for the vertical velocity, w . They assumed that w was a constant equal to the melt rate. However this is an overestimate since $w = 0$ at the lower surface. Myers et al. [15] suggested that the average value of w across the melt layer would serve as a better approximation. Yoo et al. [17] adopted a similar approach, but retained the full expression for w . They thus obtained a solution for the liquid temperature in terms of an exponential integral, which was evaluated numerically. Several authors [18,19] extended the model to three dimensions or to include an additional melt front at the upper surface of the PCM [14,20]. Groulx and Lacroix [18] considered a convection dominated three-dimensional process and show good agreement with experiments in the early stages of the process.

Due to the moving solid–liquid interface, numerical methods are usually required to solve contact melting problems. The methods for solving contact melting (and general phase change) problems are typically categorised into two groups based on their grid which can be fixed or adaptive [21,22]. The review of Dutil et al. [23] outlines a range of fixed and adaptive mesh methods that have been applied to the contact melting problem. As highlighted in Kozak and Ziskind [24], adaptive grid methods can easily deal with boundary conditions and sharp interfaces. However, they can involve complicated coordinate transformations, which are not suitable for complex geometries or three-dimensional problems. Fixed mesh methods such as the enthalpy and heat capacity methods are suited to solving melting and solidification problems. The enthalpy formulation eliminates the need to explicitly satisfy conditions at the moving interface. Hence, this method can use standard solution methods for the fluid flow and energy equations directly, without needing any mathematical transformations. Dutil et al. [23] state that the use of fixed mesh enthalpy methods simplify the problem since the governing equations are the same in both phases. Further, the interface conditions are automatically satisfied, and sharp discontinuities are avoided. They also note that due to the fact that temperature can vary with time, some studies [25] use temperature-based heat capacity methods, in which the heat equation is transformed into a nonlinear equation with a single variable. An example of a very popular fixed mesh method is that of Voller and Prakash [26] whose enthalpy–porosity fixed grid method was originally used to solve convective-diffusion phase-change problems. More recent numerical studies included additional physical effects. For example, Kozak and Ziskind [24] considered a general contact melting model that included convection in the melt layer and the sinking motion of the solid. They generated numerical solutions using a fixed-grid based on the enthalpy method and other numerical techniques including dispersed momentum sources for simulating the solid bulk and a method to move the solid across the grid whilst maintaining its rigidity. Faden et al. [27] used an enthalpy–porosity technique and a volume of fluid method to calculate the solid settling velocity. Their analysis showed good agreement between experimental data and numerical simulations for melting and settling of macro-encapsulated PCMs. Soni et al. [28] examined constrained melting of PCMs whilst paying particular attention to geometrical considerations.

A standard approximation when modelling contact melting is to assume that the material properties are temperature-invariant. Typically, this approach is applicable for small temperature changes in the system of interest. However, this is not always the case. The aim of this paper is to investigate the impact of temperature-dependent conductivity and viscosity on the contact melting process. We adopt the approach of Myers and colleagues, where the heat balance integral method (HBIM) was used to study contact melting in one [20], two [15] and three dimensions [19]. This method, originally proposed by Goodman [29], allowed the authors to remove assumptions (1), (2), (5), (6), whilst (3), (4) were shown to be reasonable, leading to small errors. Assumption (7) was neglected in [19]. In [15] the HBIM was used to obtain an approximate polynomial solution in the vertical coordinate for the temperature in the solid phase. In [19] a more accurate approximation, the opTimal Integral Method (TIM) was employed. By applying (3) in both papers an analytical approximation for the temperature in the melt layer was obtained. The solutions for the decreasing height of the PCM during melting showed excellent agreement with the experimental data of Moallemi et al. [7]. To match with the data, the two-dimensional model of [15] required a heat transfer coefficient larger than that of the three-dimensional model of [19], due to the fact that in the latter the liquid has more directions to escape.

In summary we extend the three-dimensional contact melting model of [19] by including the variation of conductivity and viscosity with temperature. To simplify the analysis we assume that both vary linearly with temperature, an assumption which is valid for sufficiently small temperature variations. We show that the temperature-dependent properties can have a significant effect on the melting process.

2. Mathematical model

We consider a cuboid PCM on a warm, flat surface held at temperature, T_s , which is greater than the PCM melt temperature, T_m . As shown in Fig. 1 the block has initial dimensions $2L \times 2B \times H_0$ such that the width is described via $x^* \in [-L, L]$, the breadth $y^* \in [-B, B]$ and the height $z^* \in [0, H_0]$, where $*$ denotes dimensional quantities. Following the experimental study of Moallemi et al. [7], the sides and top are insulated so that heat can only enter through the base. As the PCM melts, a thin liquid layer forms at the base of the PCM. This layer is squeezed by the solid, forcing the liquid to flow outwards and also ensuring that the liquid layer remains thin. Following [15,19] we divide the melting process into three stages. Stage 1 begins when the PCM is placed on the surface and ends when the lower surface of the PCM reaches the melt temperature. Typically, this stage is very short and occurs for $t^* \in [0, t_1^*]$. This is followed by stage 2, where a liquid layer exists. This stage occurs for $t^* \in [t_1^*, t_2^*]$ and ends when the temperature at the top of the PCM rises (noticeably) above the initial temperature, θ_0 . Finally, stage 3 begins at t_2^* and ends at t_3^* when the entire block is melted. The split between stages 2 and 3 is purely for mathematical reasons, and will become clear when the model is developed.

As shown in Fig. 1 the liquid layer occupies the region $z^* \in [0, h^*(t^*)]$ and the solid has height $H^*(t^*)$ with $H^*(0) = H_0$. The change in the solid height is given by $h_m^*(t^*) = H_0 - H^*(t^*)$ (note $h_m^*(t^*) \neq h^*(t^*)$ since liquid is constantly leaving the domain). The mass of the solid at any time is $M^*(t^*) = 4\rho_s LB(H_0 - h_m^*)$ where ρ_s is the solid density. In what follows the subscripts s and l represent properties related to the solid and liquid, respectively.

The aim of the typical contact melting model is to ascertain the flow of the liquid layer, and thus its height evolution. The height of the liquid depends on the melt rate, which involves the Stefan condition, which in turn depends on the temperature gradient in the both the solid and the liquid. The governing contact melting model subject to temperature-dependent conductivity and viscosity is

$$\frac{\partial}{\partial z^*} \left(\eta^*(T^*) \frac{\partial u^*}{\partial z^*} \right) = \frac{\partial p^*}{\partial x^*},$$

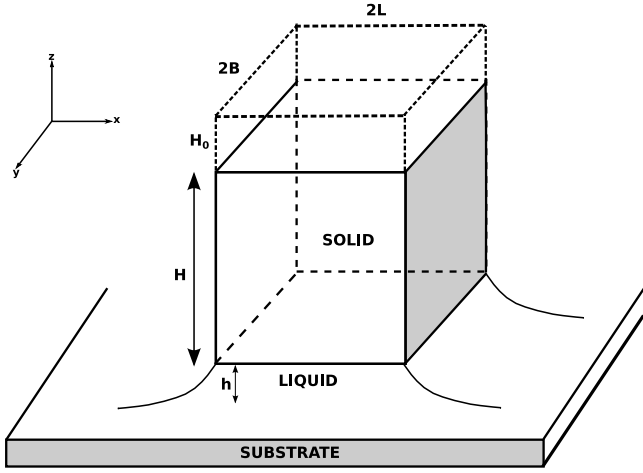


Fig. 1. Schematic of PCM floating on a liquid layer.

$$\frac{\partial}{\partial z^*} \left(\eta^*(T^*) \frac{\partial v^*}{\partial z^*} \right) = \frac{\partial p^*}{\partial y^*}, \quad \frac{\partial p^*}{\partial z^*} = 0, \quad (2.1)$$

$$\frac{\partial u^*}{\partial x^*} + \frac{\partial v^*}{\partial y^*} + \frac{\partial w^*}{\partial z^*} = 0, \quad (2.2)$$

$$0 = \frac{\partial}{\partial z^*} \left(\kappa_l^*(T^*) \frac{\partial T^*}{\partial z^*} \right), \quad (2.3)$$

$$\frac{\partial \theta^*}{\partial t^*} = \frac{\partial}{\partial z^*} \left(\kappa_s^*(\theta^*) \frac{\partial \theta^*}{\partial z^*} \right), \quad (2.4)$$

$$\rho_s L_m \frac{dh_m^*}{dt^*} = k_s^*(\theta^*) \frac{\partial \theta^*}{\partial z^*} \Big|_{z^*=h^*} - k_l^*(T^*) \frac{\partial T^*}{\partial z^*} \Big|_{z^*=h^*}, \quad (2.5)$$

The melt layer is assumed to be incompressible and since it is always thin we apply the lubrication approximation to obtain the reduced fluid flow Eqs. (2.1) [8,14,19] where (u^*, v^*, w^*) are the liquid velocities in the (x^*, y^*, z^*) directions and p^* is pressure. The viscosity $\eta^*(T^*)$ depends on the liquid temperature, T^* . In general, the largest terms neglected in (2.1) are $\mathcal{O}(\epsilon_l^2 \text{Re}) \ll 1$ where $\epsilon_l = H/L$ and Re is the standard Reynolds number. Eqs. (2.2) and (2.3) are the heat equations in the liquid and solid where θ^* is the solid temperature. The temperature-dependent thermal diffusivities are denoted $\kappa_l^*(T^*)$ and $\kappa_s^*(\theta^*)$. The liquid layer is thin throughout the melting process, and thus heat conduction in the z^* -direction dominates conduction in the x^* and y^* -directions. The convection terms are assumed negligible as they are $\mathcal{O}(\epsilon_l^2 \text{Pe}) \ll 1$ where Pe is the Peclet number. As highlighted in [9], this assumption holds true for most thermal film lubrication problems where the film is very thin. In (2.3) we only retain the conduction term in the z^* -direction because the scaling shows conduction in the x^* and y^* -directions to be small and there is no mechanism for temperature variation in the x^* and y^* -directions. This is due to the top and sides of the PCM block being insulated and the fact that the temperature of the substrate is invariant with respect to x^* and y^* . Eq. (2.4) is the Stefan condition at $z^* = h^*$, where L_m is the latent heat and $k_s^*(\theta^*)$ and $k_l^*(T^*)$ are the temperature-dependent thermal conductivities. The Stefan condition relates the motion of the film height with the heat flux across the solid-liquid interface. Finally, Eq. (2.5) is a force balance that relates the weight of the solid with the liquid pressure acting to support this weight. As in [15] we neglected the acceleration term in (2.5), which requires assuming that $H/(g\tau^2) \ll 1$ where g is gravity and τ is the relevant time scale.

The boundary conditions for the flow problem are

$$u^*|_{z^*=0} = v^*|_{z^*=0} = 0, \quad u^*|_{z^*=h^*} = v^*|_{z^*=h^*} = 0, \quad (2.6)$$

$$w^*|_{z^*=0} = 0, \quad (2.7)$$

$$w^*|_{z^*=h^*} = \frac{dh^*}{dt^*} - \frac{\rho_s}{\rho_l} \frac{dh_m^*}{dt^*}. \quad (2.8)$$

Conditions (2.6) represent no-slip at the substrate and the solid-liquid interface, whilst (2.7) denotes no-penetration at the substrate. A mass balance is used to obtain the final condition (2.8). More details of the derivation of (2.8) may be found in [19]. The pressure is ambient at the edge of the block

$$p^*|_{x^*=\pm L} = p^*|_{y^*=\pm B} = 0. \quad (2.9)$$

The thermal boundary conditions at the substrate depend on the particular stage of the melting process. Initially, contact is between two solids, and after melting has started there is liquid-solid contact. Assuming no external heat source at the substrate, we prescribe the cooling conditions

$$k_s^*(\theta^*) \frac{\partial \theta^*}{\partial z^*} = h_{ss}(\theta^* - T_S) \quad \text{at } z^* = 0, \quad (2.10)$$

$$k_l^*(T^*) \frac{\partial T^*}{\partial z^*} = h_{sl}(T^* - T_S) \quad \text{at } z^* = 0, \quad (2.11)$$

where h_{ss} and h_{sl} are the heat transfer coefficients for the pre-melt and melt stages, respectively. Condition (2.10) holds for $t^* \in [0, t_1^*]$, where t_1^* is the time the liquid appears. Once melting begins condition (2.11) applies. At the melt interface, $z^* = h^*$, we prescribe

$$\theta^* = T^* = T_m. \quad (2.12)$$

For the duration of the process the block is insulated at its upper surface, and thus

$$\frac{\partial \theta^*}{\partial z^*} \Big|_{z^*=H^*+h^*} = 0. \quad (2.13)$$

To complete the model we define the linear temperature-dependent expressions for the viscosity and thermal conductivity. For the viscosity we prescribe

$$\eta^* = \eta_0^* + \eta_1^*(T^* - T_m), \quad (2.14)$$

where the constant coefficients η_0^* and η_1^* depend on the particular PCM. For the solid and liquid thermal conductivities we define

$$k_s^*(\theta^*) = k_{s,M} + \beta'_s(\theta^* - T_m), \quad k_l^*(T^*) = k_{l,M} + \beta'_l(T^* - T_m), \quad (2.15)$$

where $k_{s,M}$ and $k_{l,M}$ are the solid and liquid conductivities, respectively, at the melt temperature. The associated thermal diffusivities are

$$\kappa_s^*(\theta^*) = \kappa_{s,M} + \beta_s(\theta^* - T_m), \quad \kappa_l^*(T^*) = \kappa_{l,M} + \beta_l(T^* - T_m), \quad (2.16)$$

where $\beta_s = \beta'_s/(\rho_s c_{p,s})$ and $\beta_l = \beta'_l/(\rho_l c_{p,l})$ and $c_{p,s}$ and $c_{p,l}$ are the constant specific heat capacities of the solid and liquid, respectively. The diffusivities of the solid and liquid at the melt temperature are denoted $\kappa_{s,M}$ and $\kappa_{l,M}$.

3. Nondimensionalisation

Nondimensionalisation is used to simplify the subsequent analysis. We define the dimensionless variables

$$t^* = \tau_m t, \quad \theta^* = T_m + (T_S - T_m)\theta, \quad T^* = T_m + (T_S - T_m)T, \quad (3.1)$$

$$x^* = Lx, \quad y^* = By, \quad z^* = H_0 z, \quad z^* = \mathcal{H}\bar{z}, \quad (3.2)$$

$$H^* = H_0 H, \quad h_m^* = H_0 h_m, \quad h^* = \mathcal{H}h, \quad (3.3)$$

$$u^* = Uu, \quad v^* = Vv, \quad w^* = Ww, \quad p^* = Pp, \quad \eta^* = \eta_M \eta, \quad (3.4)$$

where $\tau_m = H_0^2/\kappa_{s,M}$ is the melt time scale, $P = \rho_s g H_0$ is the pressure scale associated with the weight of the solid, η_M is the viscosity of the liquid at the melt temperature and \mathcal{H} is the liquid layer length scale. For the majority of the process the liquid layer is much thinner

than the solid so we define the two rescaled variables for the vertical coordinate in (3.2) where z and \bar{z} are used in the solid and liquid, respectively. From the first equation in (2.1), the velocity scale in the x direction is $U = (PH^2)/(\eta_M L)$. Similarly, the velocity scales in the y and z directions are $V = (PH^2)/(\eta_M B)$ and $W = UH/L$, respectively.

From (2.1)-(2.5) the dimensionless model is

$$\frac{\partial}{\partial \bar{z}} \left(\eta(T) \frac{\partial u}{\partial \bar{z}} \right) = \frac{\partial p}{\partial x}, \quad \frac{\partial}{\partial \bar{z}} \left(\eta(T) \frac{\partial v}{\partial \bar{z}} \right) = \frac{\partial p}{\partial y},$$

$$\frac{\partial p}{\partial \bar{z}} = 0, \quad \frac{\partial u}{\partial x} + \lambda^2 \frac{\partial v}{\partial y} + \frac{\partial w}{\partial \bar{z}} = 0, \quad (3.5)$$

$$0 = \frac{\partial}{\partial \bar{z}} \left((1 + \alpha_l T) \frac{\partial T}{\partial \bar{z}} \right), \quad (3.6)$$

$$\frac{\partial \theta}{\partial t} = \frac{\partial}{\partial z} \left((1 + \alpha_s \theta) \frac{\partial \theta}{\partial z} \right), \quad (3.7)$$

$$\frac{dh_m}{dt} = \zeta_s (1 + \alpha_s \theta) \frac{\partial \theta}{\partial z} \Big|_{z=\epsilon h} - \zeta_l (1 + \alpha_l T) \frac{\partial T}{\partial \bar{z}} \Big|_{\bar{z}=h}, \quad (3.8)$$

$$4(1 - h_m) = \int_{-1}^1 \int_{-1}^1 p \, dy \, dx, \quad (3.9)$$

where

$$\lambda = \frac{L}{B}, \quad \alpha_s = \frac{\beta_s(T_S - T_m)}{\kappa_{s,M}}, \quad \alpha_l = \frac{\beta_l(T_S - T_m)}{\kappa_{l,M}}, \quad (3.10)$$

$$\epsilon = \frac{H}{H_0}, \quad \zeta_s = \frac{k_{s,M}(T_S - T_m)}{\rho_s L_m \kappa_{s,M}}, \quad \zeta_l = \frac{k_{l,M}(T_S - T_m)}{\epsilon \rho_s L_m \kappa_{s,M}}, \quad (3.11)$$

$$\eta = \eta_0 + \eta_1 T, \quad \eta_0 = \frac{\eta_0^*}{\eta_M}, \quad \eta_1 = \frac{\eta_1^*(T_S - T_m)}{\eta_M}. \quad (3.12)$$

The vertical velocity condition at the liquid–solid interface, (2.8), becomes

$$w|_{\bar{z}=h} = A_1 \frac{dh}{dt} - A_2 \frac{dh_m}{dt}, \quad (3.13)$$

where

$$A_1 = \frac{H \kappa_{s,M}}{W H_0^2}, \quad A_2 = \frac{\rho_s \kappa_{s,M}}{\rho_l W H_0}. \quad (3.14)$$

From (2.10) and (2.11) the thermal conditions at the substrate in stages 1 and 2 become

$$(1 + \alpha_s \theta) \frac{\partial \theta}{\partial z} \Big|_{z=0} = \text{Bi}_{ss}(\theta|_{z=0} - 1), \quad (1 + \alpha_l T) \frac{\partial T}{\partial \bar{z}} \Big|_{\bar{z}=0} = \text{Bi}_{sl}(T|_{\bar{z}=0} - 1), \quad (3.15)$$

where

$$\text{Bi}_{ss} = \frac{H_0 h_{ss}}{k_{s,M}}, \quad \text{Bi}_{sl} = \frac{H h_{sl}}{k_{l,M}}. \quad (3.16)$$

From (2.13) the condition at the upper surface is

$$\frac{\partial \theta}{\partial z} \Big|_{z=\epsilon h+H} = 0. \quad (3.17)$$

Finally, the dimensionless conditions at the melt interface are

$$\theta = 0 \quad \text{at } z = \epsilon h, \quad T = 0 \quad \text{at } \bar{z} = h. \quad (3.18)$$

4. Flow in the liquid layer

The description of the liquid flow is similar to that in [19] with the main difference here being the temperature-dependent viscosity. In the limit of constant viscosity our model reduces to that of [19]. Integrating the first two equations in (2.1) and applying no-slip, no-penetration and continuity of mass flux yields

$$u = p_x \int_0^{\bar{z}} \frac{\bar{s} - hF}{\eta(\bar{s})} d\bar{s}, \quad v = p_y \int_0^{\bar{z}} \frac{\bar{s} - hF}{\eta(\bar{s})} d\bar{s}, \quad (4.1)$$

where $\eta(\bar{s}) = \eta(T(\bar{s}))$ and

$$F = \frac{1}{h} \frac{\int_0^h \bar{z}/\eta(\bar{z}) d\bar{z}}{\int_0^h 1/\eta(\bar{z}) d\bar{z}}, \quad (4.2)$$

can be viewed as the average relative fluidity of the liquid layer. Substituting (4.1) into the continuity Eq. (3.5) leads to

$$\frac{\partial w}{\partial \bar{z}} = \nabla^2 p \int_0^{\bar{z}} \frac{hF - \bar{s}}{\eta(\bar{s})} d\bar{s}, \quad (4.3)$$

where $\nabla^2 = \partial_{xx} + \lambda^2 \partial_{yy}$ is the modified Laplacian operator. Integrating the above expression across the height of the liquid layer $\bar{z} \in [0, h]$ and applying (3.13) yields

$$A_1 \frac{dh}{dt} - A_2 \frac{dh_m}{dt} = \nabla^2 p \int_0^h \int_0^{\bar{z}} \frac{hF - \bar{s}}{\eta(\bar{s})} d\bar{s} d\bar{z}. \quad (4.4)$$

Eq. (4.4) may be reformulated as a form of Poisson's equation

$$\nabla^2 p = f(t)/\xi, \quad (4.5)$$

where

$$f(t) = A_1 \frac{dh}{dt} - A_2 \frac{dh_m}{dt}, \quad \xi = \int_0^h \int_0^{\bar{z}} \frac{hF - \bar{s}}{\eta(\bar{s})} d\bar{s} d\bar{z}. \quad (4.6)$$

The latter expression can be rewritten by reversing the order of integration to give

$$\xi = \int_0^h \int_{\bar{s}}^h \frac{hF - \bar{s}}{\eta(\bar{s})} d\bar{z} d\bar{s} = h \int_0^h \frac{(hF - \bar{s})}{\eta(\bar{s})} d\bar{s} - \int_0^h \frac{\bar{s}(hF - \bar{s})}{\eta(\bar{s})} d\bar{s}, \quad (4.7)$$

which is integrated numerically in the following sections.

Eq. (4.4) may be solved via the same eigenfunction expansion used in [19], to give an infinite series solution for the pressure field. Noting that, except close to $t = 0$, the terms in the series solution decay rapidly, hence it is only necessary to retain the first term. The resulting solution for p is then substituted into the force balance (3.9) which upon integration with respect to x and y leads to

$$(1 - h_m) \frac{\xi}{\Phi} = f(t), \quad (4.8)$$

where the negative constant,

$$\Phi \approx -\frac{32}{\pi^5} \left(\pi + \frac{2(1 - \cosh \pi/\lambda)}{\sinh \pi/\lambda} \right), \quad (4.9)$$

comes from the first term of the eigenfunction expansion.

5. Thermal problem

5.1. Stage 1

The studies [15,19] used the heat balance integral method (HBIM) to solve for the solid temperature in stage 1. The method consists of the following three steps [30]. Firstly, a temperature penetration depth, $\delta(t)$, is introduced. For $z \geq \delta$ the change in temperature above the initial temperature is negligible. The position of δ is determined by imposing $\theta(\delta, t) = 0$, and to ensure a smooth transition to the initial temperature value we prescribe $\theta_z(\delta, t) = 0$. Next, a function, typically a polynomial, is used to approximate the temperature profile. Finally, the heat equation is integrated to obtain the so-called heat balance integral.

Both [15,19] observed that the pre-melt stage was very short. For example, in the three-dimensional study of [19], stage 1 only represented approximately $10^{-4}\%$ of the total melt process for n-octadecane. Thus, we neglect the details of stage 1 here and use the appropriate expressions from [19]. Specifically, we require t_1 to be the time when melting at the lower surface begins and the associated position of the penetration depth to be δ_1 . Applying the dimensionless variables from here to (34) and (35) from [19] yields

$$t_1 = \frac{1}{m(m+1)} \left[\frac{\delta_1^2}{2} + \frac{m}{\text{Bi}_{ss}} \delta_1 - \frac{m^2}{\text{Bi}_{ss}^2} \ln \left(1 + \frac{\text{Bi}_{ss}}{m} \delta_1 \right) \right],$$

$$\delta_1 = \frac{m(T_m - \theta_0)}{\text{Bi}_{ss}(T_S - T_m)}. \quad (5.1)$$

In previous contact melting HBIM treatments [9,15] the values $m = 2, 3$ were used. Myers [31] developed a systematic approach for selecting

the exponent that minimises the error in the temperature profile, based on a least-squares calculation. This is termed the opTimal Integral Method or TIM. For the present case of a Newton cooling condition, from [31] the appropriate value is $m = 3.58$. This was subsequently used in the contact melting study [19], and will also be used in the current analysis.

5.2. Stage 2

In stage 2 the heat equations in the liquid and solid, (3.6) and (3.7), must both be solved. Firstly, integrating the heat equation for the liquid temperature yields

$$T + \alpha_l \frac{T^2}{2} = \text{Bi}_{sl}(T_0 - 1)(\bar{z} - h), \quad (5.2)$$

with solution

$$T = \frac{-1 + \sqrt{1 + 2\alpha_l \text{Bi}_{sl}(T_0 - 1)(\bar{z} - h)}}{\alpha_l}, \quad (5.3)$$

where $T_0 = T(0, t)$ is the dimensionless liquid temperature at the substrate and is obtained by evaluating (5.2) at $\bar{z} = 0$ to give

$$T_0 = \frac{-(1 + \text{Bi}_{sl}h) + \sqrt{(1 + \text{Bi}_{sl}h)^2 + 2\alpha_l \text{Bi}_{sl}h}}{\alpha_l}. \quad (5.4)$$

To check that we have selected the correct root in (5.3) we multiply (5.4) by the conjugate of its numerator to obtain

$$T_0 = \frac{2\text{Bi}_{sl}h}{1 + \text{Bi}_{sl}h + \sqrt{(1 + \text{Bi}_{sl}h)^2 + 2\alpha_l \text{Bi}_{sl}h}}. \quad (5.5)$$

As time increases, the film thickness also increases and the temperature of the liquid at $\bar{z} = 0$ approaches the substrate temperature. Upon inspecting the limiting behaviour of (5.5) as $t \rightarrow \infty$, and thus $h \rightarrow \infty$ we obtain $T_0 \rightarrow 1$, or in dimensional terms $T_0^* \rightarrow T_S^*$.

In the solid we apply the HBIM and assume a temperature profile of the form

$$\theta(z, t) = a_0 + a_1 \left(\frac{\delta - z}{\delta - \epsilon h} \right) + a_n \left(\frac{\delta - z}{\delta - \epsilon h} \right)^n. \quad (5.6)$$

Upon applying the dimensionless conditions $\theta(\epsilon h, t) = 0$, $\theta(\delta, t) = \Delta\theta \equiv (\theta_0 - T_m)/(T_S - T_m)$ and $\theta_z(\delta, t) = 0$ we obtain

$$\theta(z, t) = \Delta\theta - \Delta\theta \left(\frac{\delta - z}{\delta - \epsilon h} \right)^n. \quad (5.7)$$

The value of the exponent n is fixed via a similar argument as that used in stage 1. In stage 2 the base of the solid is now fixed at the melt temperature, and thus for this type of boundary condition $n = 2.235$ minimises the least squares error [31].

To obtain the heat balance integral we integrate the heat equation in the solid across $z \in [\epsilon h, \delta]$ to give

$$\frac{d\delta}{dt} = -n\epsilon \frac{dh}{dt} + \frac{n(n+1)}{\delta - \epsilon h}. \quad (5.8)$$

Substituting the appropriate expressions for the temperature gradients into the Stefan condition (3.8) yields

$$\frac{dh_m}{dt} = \frac{\zeta_s n \Delta\theta}{\delta - \epsilon h} - \zeta_l \text{Bi}_{sl}(T_0 - 1). \quad (5.9)$$

The final equation required to close the system is the force balance (4.8), which requires numerical evaluation of the integral ξ in (4.7).

To summarise, the system of three first-order differential Eqs. (4.8), (5.8) and (5.9) are solved numerically. The associated initial conditions are $\delta(t_1) = \delta_1$, $h(t_1) = h_m(t_1) = 0$. The solutions are continued until the heat has penetrated through the entire PCM so that $\delta = h + H$, which then fixes the time t_2 . The values $h(t_2) = h_2$ and $h_m(t_2) = h_{m2}$ are then used as initial conditions for stage 3.

Table 1

Typical parameters values for solid/liquid n-octadecane.

Symbol	Value	Units
L, B, H_0	0.0175, 0.115, 0.055	m [7]
H	0.0001	m [10,15]
g	9.8	m s ⁻²
ρ_s, ρ_l	930, 771.2	kg m ⁻³ [19]
$c_{p,s}, c_{p,l}$	2151, 2161	m ² s ⁻² K ⁻¹ [7]
$k_{s,M}, k_{l,M}$	0.3723, 0.15	W m ⁻¹ K ⁻¹ [19]
$\kappa_{s,M}, \kappa_{l,M}$	1.9×10^{-7} , 9×10^{-8}	m ² s ⁻¹ [19]
β_s, β_l	-7.7×10^{-11} , -2.1×10^{-10}	m ² s ⁻¹ K ⁻¹ [32]
β'_s, β'_l	-1.5×10^{-4} , -3.6×10^{-4}	kg m s ⁻³ K ⁻² [32]
η_M, η_0	0.0036, 0.004	N s m ⁻² [19]
η_l	-4×10^{-4}	N s m ⁻² K ⁻¹ [32]
L_m	2.435×10^5	J kg ⁻¹ [7]
T_S, T_m, θ_0	308.2, 301.33, 298	K [7]
h_{ss}, h_{sl} (Constant properties)	5740, 5740	W m ⁻² K ⁻¹
h_{ss}, h_{sl} (Variable properties)	6250, 6250	W m ⁻² K ⁻¹

5.3. Stage 3

In the final stage the solution for the liquid temperature remains the same as that in stage 2. In the solid, the entire PCM is above the initial solid temperature, θ_0 , and hence, the penetration depth is no longer applicable. Instead we define a new unknown which is the temperature at the upper surface of the block. This surface is insulated so we prescribe $\theta_z(\epsilon h + H, t) = 0$ and $\theta(\epsilon h + H, t) = \theta_H(t)$ where θ_H is to be determined. At the lower surface, at the liquid–solid interface, we retain $\theta(\epsilon h, t) = 0$, and hence the temperature is expressed as

$$\theta(z, t) = \theta_H - \theta_H \left(\frac{\epsilon h + H - z}{H} \right)^n, \quad (5.10)$$

where again $n = 2.235$.

Applying a standard HBI results in a complicated expression for θ_H . To simplify this type of analysis Goodman [29] proposed a dimensional function, ϕ^* , defined as the integral of the temperature over the domain of interest,

$$\phi^* = \int_{h^*}^{h^*+H^*} \theta^* dz^*, \quad (5.11)$$

The above quantity has units K m, and thus rescaling via the change of variable $\phi^* = \phi H_0(T_S - T_m)$ leads to

$$\phi = \int_{\epsilon h}^{\epsilon h+H} (\theta + \Delta\theta_1) dz = H \left(\Delta\theta_1 + \frac{n\theta_H}{n+1} \right), \quad (5.12)$$

where $\Delta\theta_1 = T_m/(T_S - T_m)$. Expression (5.12) is rearranged to give

$$\theta_H = \frac{n+1}{n} \left(\frac{\phi}{H} - \Delta\theta_1 \right). \quad (5.13)$$

Next we integrate the heat equation in the solid over $z \in [\epsilon h, \epsilon h + H]$ to give an equation for ϕ :

$$\frac{d\phi}{dt} = -(\Delta\theta_1 + \theta_H) \frac{dh_m}{dt} + \epsilon \theta_H \frac{dh}{dt} - \frac{n\theta_H}{1-h_m}. \quad (5.14)$$

From (3.8) the Stefan condition in this stage is

$$\frac{dh_m}{dt} = \frac{n\zeta_s \theta_H}{1-h_m} - \zeta_l \text{Bi}_{sl}(T_0 - 1). \quad (5.15)$$

The problem in stage 3 consists of solving three first-order differential equations, namely the force balance (4.8), (5.14) and the Stefan condition (5.15). The associated initial conditions are $h(t_2) = h_2$, $h_m(t_2) = h_{m2}$ and continuity of temperature requires $\theta_H(t_2) = \Delta\theta$. Via (5.12), the final condition is equivalent to

$$\phi(t_2) = (1 - h_{m2}) \left(\Delta\theta_1 + \frac{n\Delta\theta}{n+1} \right). \quad (5.16)$$

The process ends at t_3 when $h_m = 1$ and the solid has melted completely.

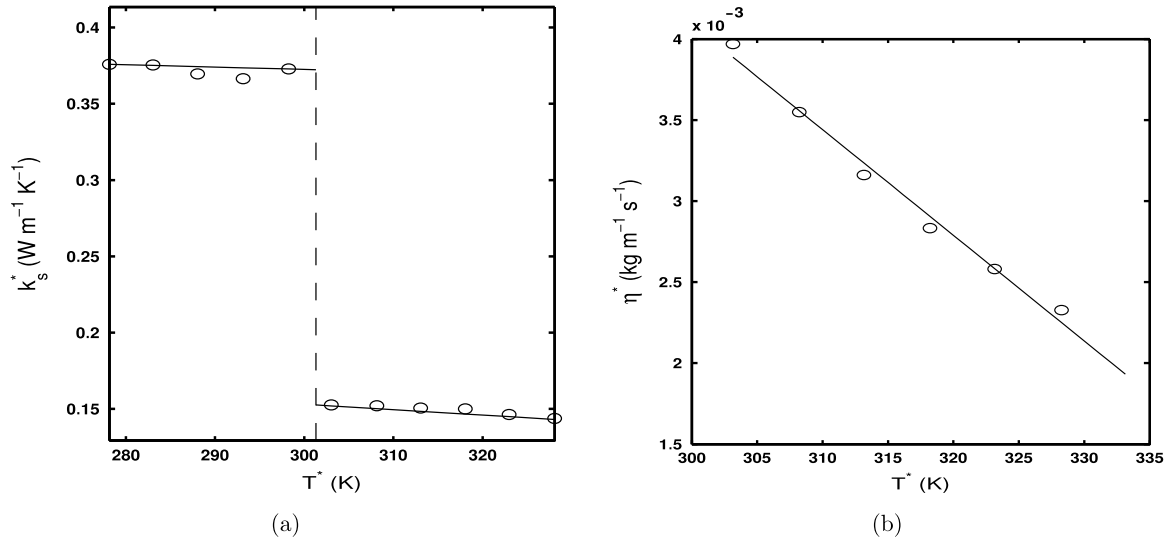


Fig. 2. Experimental data of Motahar et al. [32] for n-octadecane (circles) against linear fits (solid line) for (a) thermal conductivity and (b) viscosity.

6. Results

The solutions obtained in the previous sections are used to describe the melting of n-octadecane, taking into account the temperature-dependent properties. This PCM material was chosen because there is a great deal of data concerning its thermophysical properties as well as good experimental data for the melting process [7]. This data was employed in the theoretical studies of [15,19,20]. Further, Motahar et al. [32] investigated the effect of temperature on the thermal conductivity and viscosity of n-octadecane, so we can easily describe their variation with temperatures.

The study of Moallemi et al. [7] involved placing a block of n-octadecane, initially at 298 K, on a flat surface maintained at 308.2 K. The sides and top of the block were insulated, so heat transfer only occurred at the base. The typical height scale, $H = 0.1$ mm, follows the theoretical and experimental studies [10,15]. Values for the thermophysical parameters, and the dimensions of the block, are summarised in Table 1. Fig. 2 shows the experimentally determined values for the dimensional variation of conductivity and viscosity with temperature [32]. Data points are represented by circles, the solid lines show linear fits: the appropriate values of β and η required for the linear relations (2.14) and (2.15) are also shown in Table 1. The jump in conductivity at 301.33 K represents the jump between solid and liquid values. Within each phase the conductivity showed little variation, while the viscosity decreased by a factor 2 during the experiment.

The final unknown values for the simulation are the heat transfer coefficients h_{ss} and h_{sl} . In stage 1 we assume that $h_{ss} = h_{sl}$ as this stage is short compared to the length of the total melting process. We approximate h_{sl} using the approach in [33] to study droplet evaporation on a hot surface. The same approach was also used in the contact melting studies [15,19]. Fig. 3 compares our numerical solution for the solid height (solid line) with the corresponding experimental data (circles) from [7]. In our simulation h_{sl} is the only unknown parameter we are free to choose. Using a least squares fitting method in Matlab we obtain $h_{sl} = 6250$ W m⁻² K⁻¹. Fig. 3 shows that using this value of h_{sl} leads to excellent agreement between the data and our simulation. We can be confident that this choice of h_{sl} is accurate as an incorrect model with a single free parameter would be unlikely to match the data points as well as shown in the graph. Further, in Fig. 3 we show the effect of using different values of h_{sl} . The dashed dotted and dashed lines represent numerical solutions for $h_{sl} = 8750$ W m⁻² K⁻¹ and $h_{sl} = 3750$ W m⁻² K⁻¹, respectively. The curves shows that, as expected, a higher heat transfer coefficient leads to quicker melting, whilst a lower heat transfer coefficient leads to longer melting.

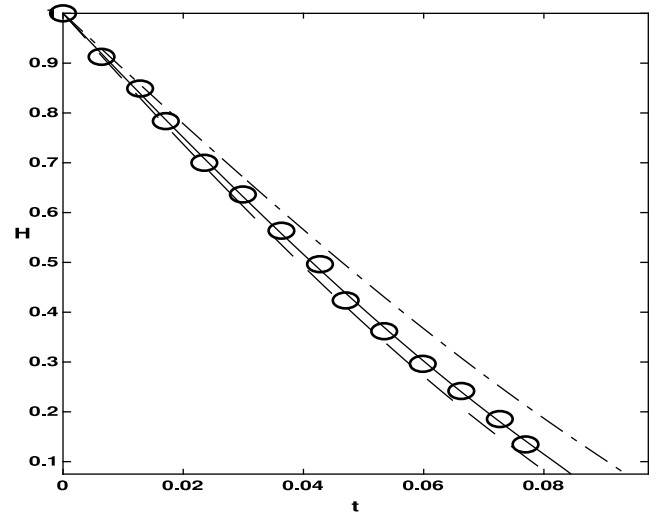


Fig. 3. Comparison of experimental data (circles) from [7] with our numerical solution subject to $h_{sl} = 6250$ W m⁻² K⁻¹ (solid line), $h_{sl} = 8750$ W m⁻² K⁻¹ (dashed line) and $h_{sl} = 3750$ W m⁻² K⁻¹ (dash dotted line).

As highlighted in Section 5.1, the pre-melt stage amounts to a small fraction of the total process. For n-octadecane, via the first expression in (5.1), stage 1 ends after $t_1^* = 0.0029$ s. Due to the short duration of this stage, the temperature-dependent solid thermal conductivity is not expected to affect melting. Supporting this observation is the fact that, in the case of n-octadecane at least, the solid conductivity does not exhibit significant variation with temperature.

Fig. 4 shows the evolution of the liquid height subject to temperature-dependent properties. The liquid height varies qualitatively in the same way to that of the constant property case of [19]. When melting first starts there is an initial rapid rise in the layer thickness. This is followed by a slow increase and finally a rapid rise when the solid weight is not sufficient to squeeze the liquid outwards. However, for the constant property case in [19] excellent agreement was also obtained. The key difference between the two sets of results lies in the heat transfer coefficient. The model of [19] requires $h_{sl} = 5740$ W/(m² K). We note that there was a mistake in [19] concerning the width of the block, which was taken to be $B = 0.0175$ m whereas the actual value in the experiment was 0.115 m. Thus, the corrected

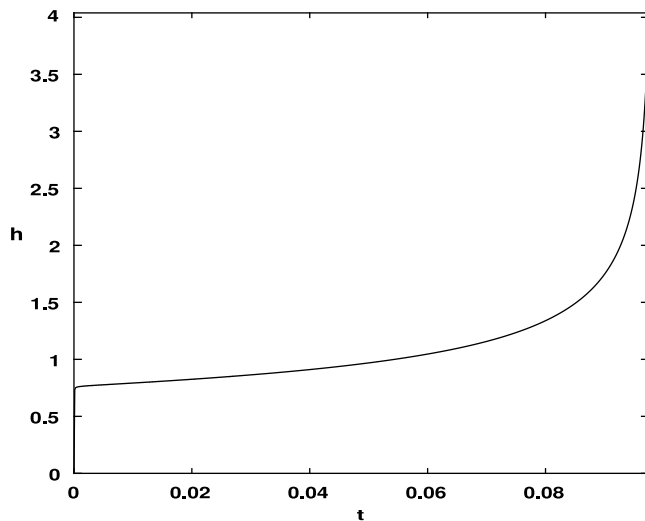


Fig. 4. Numerical simulation for liquid height subject to temperature-dependent properties.

heat transfer coefficient is $h_{sl} = 5740 \text{ W m}^{-2} \text{ K}^{-1}$, and not the original value $3275 \text{ W m}^{-2} \text{ K}^{-1}$ in [19]. The current model has $h_{sl} = 6250 \text{ W/(m}^2 \text{ K)}$, an approximately 10% increase. The fact that we now require a higher heat transfer coefficient to achieve melting in the same time indicates that taking account of the variable material properties in fact leads to a slower melt process than the constant property model. This result is unexpected given that there is a large decrease in viscosity with temperature which results in a thinner liquid layer. This should allow the heat from the substrate to penetrate the solid more rapidly and so significantly decrease the melt time. This effect is clearly offset by the decrease in thermal conductivity with temperature, resulting in only a slight change in the heat transfer coefficient. However, numerical simulations demonstrate that if only one of these effects is included then the melt times change dramatically. The close agreement of previous models, which involve constant parameter values, is therefore fortuitous: the two dominant thermally varying parameters largely cancel each other out making previous models appear more accurate than in reality.

To examine the melt process further, we varied the coefficients in the expressions for the viscosity and liquid conductivity. Firstly, we examine the effect of changing η_l , the slope in the viscosity expression, whilst keeping the other parameters fixed. A decrease in the slope causes the viscosity to decrease more rapidly with increasing temperature. Fig. 5(a) shows the liquid height for constant viscosity (solid line) and our solution for the original value of η_l (dashed line) and $8\eta_l$ (dotted line). As the slope in the viscosity expression becomes increasingly negative, and thus the viscosity decreases more rapidly with temperature, the melt time also decreases. This can be explained by the fact that the decrease in viscosity with temperature leads to the melt layer flowing more rapidly from beneath the PCM. This leads to a thinner layer which provides less resistance to heat transfer across the liquid, and hence the shorter melt times. Fig. 5(b) shows the liquid height for constant liquid conductivity (solid line) and our solution for the original value of β'_l (dashed line) and β'_l multiplied by factors of 10 (dotted line) and -10 (dash dotted line). Multiplying β'_l (which we recall is negative) by the negative factor causes the liquid conductivity to increase quicker with increasing temperature. This leads to improved heat transfer across the liquid layer, and hence more rapid melting as indicated by the dash dotted line in the graph.

7. Conclusion

The goal of this paper was to investigate the effect of temperature-dependent material properties on the melting of a PCM. We extended

the three-dimensional model of [19] to include thermal conductivity and viscosity that both vary linearly with temperature. The analysis made it clear that significant variations in the melt time are possible due to temperature-dependent effects. However, in the specific case examined, using the experimental data for n-octadecane [7,32], results were not very far removed from the constant property solutions of previous models. This was due to a competition between the decrease in viscosity and conductivity. The accuracy of previous results was therefore fortuitous since although both effects lead to a significant variation in melt times, taken together they almost cancel each other out. So, for the n-octadecane experiments of [7] a constant property model gives reasonable results provided an appropriate heat transfer coefficient is chosen.

Although the mathematical description of the present model appears relatively complex (in comparison to previous models for PCM melting) the information required for Stage 1 is given as an algebraic formulae. Stages 2 and 3 involve solving three coupled first-order ordinary differential equations. This is a much simpler task than the solution of the original system consisting of a partial differential equation system for the liquid flow, coupled to heat equations in the liquid and solid, and all to be solved over an unknown, moving domain. The ordinary differential equations can be easily solved via ordinary differential equation routines in Matlab.

Several extensions to our research will be addressed in future studies. One obvious extension is to reexamine the model with properties that vary nonlinearly with respect to temperature. For example, temperature-dependent viscosity has been described using nonlinear empirical models including exponential and Arrhenius models. However, the inclusion of such expressions would make our study more complex. In a future study we will also consider how our analysis can be used to assist in the selection of PCMs with temperature-dependent properties which are best suited for a particular application. For instance, n-octadecane shares a problem common to many other organic PCMs [34], namely low thermal conductivity [35,36]. This can have a detrimental effect on the performance of latent heat storage systems, which require high energy release rates. Fluid properties may be altered by the addition of nanoparticles, this leads to nanoparticle-enhanced phase change materials (NEPCM) [37–39]. The addition of nanoparticles has the potential to change the thermal properties and viscosity of the liquids. Effectively then, our analysis could be used to tune PCM properties and look for more efficient energy storage materials. For example, our study demonstrated that a decrease in the liquid conductivity leads to longer melting times. This is a desirable property for cooling applications because as the PCMs melt, they absorb energy with almost no change in temperature. Hence, in this scenario PCMs with long melting times are preferable. On the other hand, if quick energy release is the goal, it would be desirable to design a material where the viscosity decreases with temperature while the conductivity increases.

Declaration of competing interest

The authors declare that they have no known competing financial interests or personal relationships that could have appeared to influence the work reported in this paper.

Acknowledgements

V. Cregan was supported by a “la Caixa” foundation, Spain grant and a European Cooperation in Science and Technology, Spain Short Term Short Mission grant (COST action TD1409, STSM reference number 41265). T. G. Myers acknowledges financial support from the Ministerio de Ciencia e Innovación, Spain Grant No. MTM2017-82317-P.

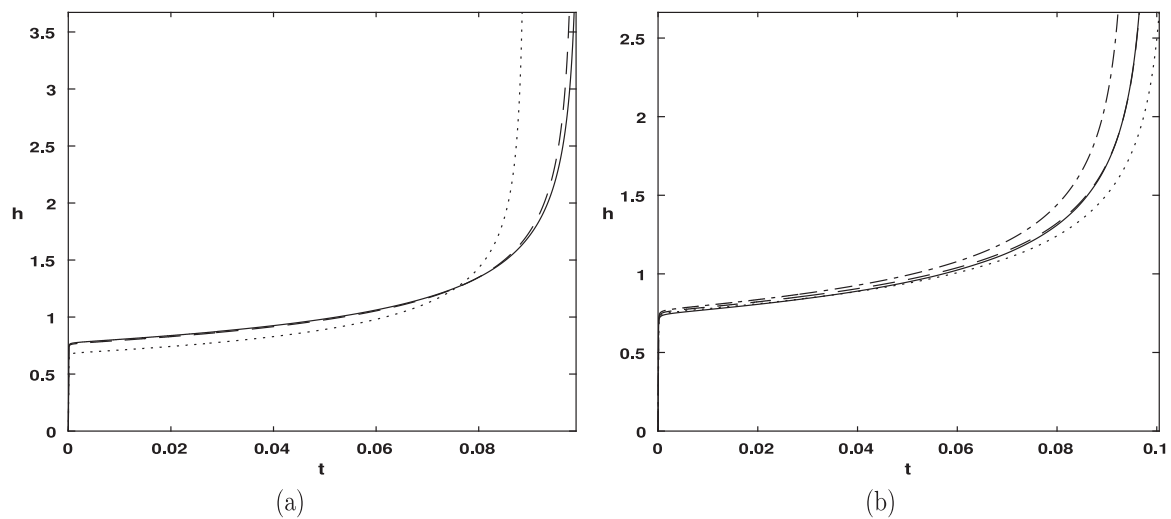


Fig. 5. Liquid height in stages 2 and 3 subject to (a) constant viscosity (solid line) and temperature-dependent viscosity for original value of η_1 from data (dashed line) and $8\eta_1$ (dotted line) (b) Liquid height in stages 2 and 3 subject to constant liquid conductivity (constant line) and temperature-dependent liquid conductivity for original value of β'_1 from data (dashed line), $10\beta'_1$ (dotted line) and $-10\beta'_1$ (dash dotted line).

References

- [1] A.M. Khudhair, M.M. Farid, A review on energy conservation in building applications with thermal storage by latent heat using phase change materials, *Energy Convers. Manage.* 45 (2) (2004) 263–275.
- [2] D. Zhou, C.Y. Zhao, Y. Tian, Review on thermal energy storage with phase change materials (PCMs) in building applications, *Appl. Energy* 92 (2012) 593–605.
- [3] S. Mondal, Phase change materials for smart textiles—an overview, *Appl. Therm. Eng.* 28 (11) (2008) 1536–1550.
- [4] H. Shim, E.A. McCullough, B.W. Jones, Using phase change materials in clothing, *Textile Res. J.* 71 (6) (2001) 495–502.
- [5] M. Kenisarin, K. Mahkamov, Solar energy storage using phase change materials, *Renew. Sustain. Energy Rev.* 11 (9) (2007) 1913–1965.
- [6] A. Shukla, D. Buddhi, R.L. Sawhney, Solar water heaters with phase change material thermal energy storage medium: A review, *Renew. Sustain. Energy Rev.* 13 (8) (2009) 2119–2125.
- [7] M.K. Moallemi, B.W. Webb, R. Viskanta, An experimental and analytical study of close-contact melting, *J. Heat Transfer* 108 (4) (1986) 894–899.
- [8] A. Bejan, The fundamentals of sliding contact melting and friction, *J. Heat Transfer* 111 (1) (1989) 13–20.
- [9] A. Bejan, Contact melting heat transfer and lubrication, *Adv. Heat Transfer* 24 (1994) 1–38.
- [10] T. Hirata, Y. Makino, Y. Kaneko, Analysis of close-contact melting for octadecane and ice inside isothermally heated horizontal rectangular capsule, *Int. J. Heat Mass Transfer* 34 (12) (1991) 3097–3106.
- [11] P.A. Litsek, A. Bejan, Sliding contact melting: the effect of heat transfer in the solid parts, *J. Heat Transfer* 112 (3) (1990) 808–812.
- [12] H. Hong, A. Saito, Numerical method for direct contact melting in transient process, *Int. J. Heat Mass Transfer* 36 (8) (1993) 2093–2103.
- [13] H. Yoo, Analytical solutions to the unsteady close-contact melting on a flat plate, *Int. J. Heat Mass Transfer* 43 (8) (2000) 1457–1467.
- [14] M. Lacroix, Contact melting of a phase change material inside a heated parallelepiped capsule, *Energy Convers. Manage.* 42 (1) (2001) 35–47.
- [15] T.G. Myers, S.L. Mitchell, G. Muchatibaya, Unsteady contact melting of a rectangular cross-section material on a flat plate, *Phys. Fluids* 20 (10) (2008) 103101.
- [16] D. Groulx, M. Lacroix, Study of close contact melting of ice from a sliding heated flat plate, *Int. J. Heat Mass Transfer* 49 (23) (2006) 4407–4416.
- [17] H. Yoo, H. Hong, C.J. Kim, Effects of transverse convection and solid-liquid density difference on the steady close-contact melting, *Int. J. Heat Fluid Flow* 19 (4) (1998) 368–373.
- [18] D. Groulx, M. Lacroix, Study of the effect of convection on close contact melting of high Prandtl number substances, *Int. J. Therm. Sci.* 46 (3) (2007) 213–220.
- [19] M.M. MacDevette, T.G. Myers, Contact melting of a three-dimensional phase change material on a flat substrate, *Int. J. Heat Mass Transfer* 55 (23) (2012) 6798–6807.
- [20] T.G. Myers, S.L. Mitchell, G. Muchatibaya, M.Y. Myers, A cubic heat balance integral method for one-dimensional melting of a finite thickness layer, *Int. J. Heat Mass Transfer* 50 (25) (2007) 5305–5317.
- [21] M. Lacroix, Modeling of latent heat storage systems, in: *Thermal Energy Storage Systems and Applications*, John Wiley & Sons Chichester, 2002.
- [22] M. Lappa, *Fluids, Materials and Microgravity: Numerical Techniques and Insights into Physics*, Elsevier, 2004.
- [23] Y. Dutil, D.R. Rousse, N.B. Salah, S. Lassue, L. Zalewski, A review on phase-change materials: mathematical modeling and simulations, *Renew. Sustain. Energy Rev.* 15 (1) (2011) 112–130.
- [24] Y. Kozak, G. Ziskind, Novel enthalpy method for modeling of PCM melting accompanied by sinking of the solid phase, *Int. J. Heat Mass Transfer* 112 (2017) 568–586.
- [25] Y. Cao, A. Faghri, A numerical analysis of phase-change problems including natural convection, *Trans. ASME C* 112 (3) (1990).
- [26] V.R. Voller, C. Prakash, A fixed grid numerical modelling methodology for convection-diffusion mushy region phase-change problems, *Int. J. Heat Mass Transfer* 30 (8) (1987) 1709–1719.
- [27] M. Faden, A. König-Haagen, S. Höhle, D. Brüggemann, An implicit algorithm for melting and settling of phase change material inside macrocapsules, *Int. J. Heat Mass Transfer* 117 (2018) 757–767.
- [28] V. Soni, A. Kumar, V.K. Jain, Modeling of PCM melting: Analysis of discrepancy between numerical and experimental results and energy storage performance, *Energy* 150 (2018) 190–204.
- [29] T.R. Goodman, The heat-balance integral and its application to problems involving a change of phase, *Trans. ASME* 80 (2) (1958) 335–342.
- [30] S.L. Mitchell, T.G. Myers, Application of standard and refined heat balance integral methods to one-dimensional Stefan problems, *SIAM Rev.* 52 (1) (2010) 57–86.
- [31] T. Myers, Optimizing the exponent in the heat balance and refined integral methods, *Int. Commun. Heat Mass Transfer* 36 (2) (2009) 143–147.
- [32] S. Motahar, N. Nikkam, A.A. Alemrajabi, R. Khodabandeh, M.S. Toprak, M. Muhammed, A novel phase change material containing mesoporous silica nanoparticles for thermal storage: a study on thermal conductivity and viscosity, *Int. Commun. Heat Mass Transfer* 56 (2014) 114–120.
- [33] T.G. Myers, J.P.F. Charpin, A mathematical model of the leidenfrost effect on an axisymmetric droplet, *Phys. Fluids* (1994-present) 21 (6) (2009) 063101.
- [34] L. Fan, J.M. Khodadadi, Thermal conductivity enhancement of phase change materials for thermal energy storage: a review, *Renew. Sustain. Energy Rev.* 15 (1) (2011) 24–46.
- [35] R. Velraj, R.V. Seeniraj, B. Hafner, C. Faber, K. Schwarzer, Heat transfer enhancement in a latent heat storage system, *Sol. Energy* 65 (3) (1999) 171–180.
- [36] M. Xiao, B. Feng, K. Gong, Preparation and performance of shape stabilized phase change thermal storage materials with high thermal conductivity, *Energy Convers. Manage.* 43 (1) (2002) 103–108.
- [37] C.J. Ho, J.Y. Gao, Preparation and thermophysical properties of nanoparticle-in-paraffin emulsion as phase change material, *Int. Commun. Heat Mass Transfer* 36 (5) (2009) 467–470.
- [38] Y.D. Liu, Y.G. Zhou, M.W. Tong, X.S. Zhou, Experimental study of thermal conductivity and phase change performance of nanofluids PCMs, *Microfluid. Nanofluid.* 7 (4) (2009) 579–584.
- [39] M.M. MacDevette, T.G. Myers, Nanofluids: An innovative phase change material for cold storage systems? *Int. J. Heat Mass Transfer* 92 (2016) 550–557.